

GaN/SiO<sub>2</sub> interface that does not create states within the band gap: A theoretical predictionKengo Nishio<sup>1</sup>,\* Takehide Miyazaki, and Mitsuaki Shimizu*National Institute of Advanced Industrial Science and Technology (AIST), Central 2, Umezono 1-1-1, Tsukuba, Ibaraki 305-8568, Japan* (Received 23 December 2020; revised 27 July 2021; accepted 26 August 2021; published 1 October 2021)

For the application of GaN to power transistors, we theoretically search for the interface between GaN and amorphous SiO<sub>2</sub> (*a*-SiO<sub>2</sub>) that meets the following requirements: (1) both the conduction band minimum and valence band maximum originate from the GaN (straddling band gap) and (2) the formation of states in the band gap of the GaN is minimized. To this end, we first show that an epitaxial silica bilayer on *m*-plane GaN (*m*-GaN) meets these requirements when the GaN surface is doped with zinc and oxygen. By using this epitaxial layer as a seed, we make a structure model of the *m*-GaN/*a*-SiO<sub>2</sub> interface with a straddling gap without in-gap states. Our findings show that a key determinant of the nature of *m*-GaN/*a*-SiO<sub>2</sub> interface band structure is what we call the “contact structure,” a region of just a few atomic layers thickness at the very interface. We propose that the complex problem of designing semiconductor/insulator interfaces can be reduced to the simpler problem of designing ultrathin epitaxial insulators on the semiconductor surface.

DOI: [10.1103/PhysRevMaterials.5.104601](https://doi.org/10.1103/PhysRevMaterials.5.104601)

## I. INTRODUCTION

Interfaces between different materials are ubiquitous, and their atomic structure has been a major subject of materials science [1–3]. In metal-oxide-semiconductor field-effect transistors, a gate insulator is grown on a semiconductor surface [4]. Since the semiconductor and insulator have different atomic structure, dangling bonds are easily formed at the semiconductor/insulator interface. Such defects need to be reduced, for they create electronic states in the band gap, which degrade the performance of transistors [5].

Recently, gallium nitride (GaN) has attracted much attention because of its large band gap energy suitable for power transistors [6]. Amorphous silica (*a*-SiO<sub>2</sub>) is often used as the gate insulator in GaN-based transistors [7–9]. An experimental study has suggested that the GaN/*a*-SiO<sub>2</sub> interface has more dangling bond states near the valence band maximum (VBM) than the conduction band minimum (CBM) [10]. Therefore, the reduction of dangling bond states, ones near VBM in particular, is a challenge for the application of GaN.

To reduce the dangling bonds at the GaN/*a*-SiO<sub>2</sub> interface, knowledge about the Si/SiO<sub>2</sub> interface will be useful. Despite their different atomic structures, a high-quality interface can be formed between Si and *a*-SiO<sub>2</sub>. At the interface, an atomically thin ordered layer is formed, which serves as a buffer for smoothly connecting the different structures [11–13]. Form-

ing such a buffer layer would be key to reducing dangling bond density at the GaN/*a*-SiO<sub>2</sub> interface [14–17].

One possible approach to form an ordered buffer layer is using an atomically thin epitaxial layer as a seed [18]. An experimental study has demonstrated that an ultrathin silicon oxynitride (Si<sub>4</sub>O<sub>5</sub>N<sub>3</sub>) layer can epitaxially grow on 6H-SiC(0001) [19]. By analogy between the structure of SiC and GaN, a first-principle study has proposed that the epitaxial formation of an Si<sub>4</sub>O<sub>5</sub>N<sub>3</sub> layer is possible on *c*-plane GaN (*c*-GaN) [17]. The *c*-GaN/Si<sub>4</sub>O<sub>5</sub>N<sub>3</sub> interface does not have any dangling bonds and its CBM originates from the GaN. However, its VBM originates from the Si<sub>4</sub>O<sub>5</sub>N<sub>3</sub> layer. In other words, the *c*-GaN/Si<sub>4</sub>O<sub>5</sub>N<sub>3</sub> interface creates states in the band gap of the GaN.

The recent demonstration of GaN-based transistors with *m*-plane channels has stimulated interest in the interface between *m*-plane GaN (*m*-GaN) and *a*-SiO<sub>2</sub> [20]. The possibility has been discussed that a clean *m*-GaN surface might create dangling-bond states in the band gap of the bulk GaN [21,22] and such in-gap states could be removed by attaching hydrogen atoms to the surface Ga and N atoms [23]. However, it is unknown whether it is possible to form the *m*-GaN/*a*-SiO<sub>2</sub> interface that does not have states in the band gap. In addition, for the application of GaN to power transistors, band alignment at the GaN/insulator interface needs to be a straddling type. In other words, both CBM and VBM need to originate from the GaN. Even if an *m*-GaN/*a*-SiO<sub>2</sub> interface without in-gap states can be made, it is still nonobvious whether the interface has a straddling gap.

In this work, using first principles calculations and classical molecular dynamics simulations, we search for the *m*-GaN/*a*-SiO<sub>2</sub> interface that meets the following requirements: (1) both CBM and VBM originate from the GaN and (2) no states form in the band gap of the GaN. By following the idea that an ultrathin epitaxial insulator may serve as a seed for a structurally smooth semiconductor/insulator interface [18]

\*k-nishio@aist.go.jp

Published by the American Physical Society under the terms of the [Creative Commons Attribution 4.0 International](https://creativecommons.org/licenses/by/4.0/) license. Further distribution of this work must maintain attribution to the author(s) and the published article's title, journal citation, and DOI.

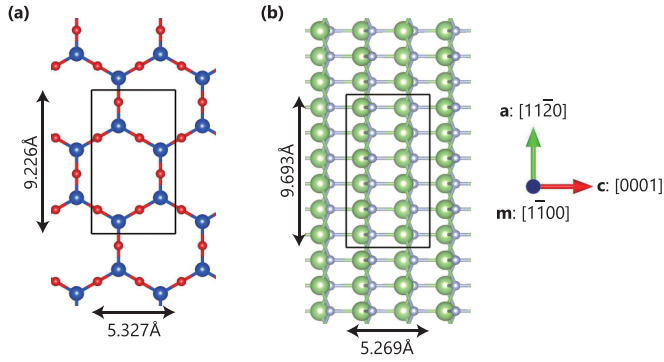


FIG. 1. Top views of (a) a freestanding  $h$ -SiO<sub>2</sub> bilayer and (b) a bulk  $m$ -GaN substrate. The blue, red, green, and gray spheres represent Si, O, Ga, and N atoms, respectively. The square represents the supercell.

and our intuition that a key determinant of the nature of interface band structure is what we call the “contact structure,” a region of just a few atomic layers thickness at the very interface, we first search for the ultrathin epitaxial silica on  $m$ -GaN that meets the two requirements. We find that an epitaxial hexagonal silica ( $h$ -SiO<sub>2</sub>) bilayer on  $m$ -GaN meets the two requirements when the GaN surface is doped with zinc and oxygen. By using this structure as a seed, we make a structurally smooth  $m$ -GaN/ $a$ -SiO<sub>2</sub> interface having the same contact structure formed in the epitaxial  $h$ -SiO<sub>2</sub> bilayer on  $m$ -GaN. The resultant interface has a straddling gap without in-gap states. Our findings demonstrate a crucial role of the contact structure played in the  $m$ -GaN/ $a$ -SiO<sub>2</sub> interface.

## II. METHODS

First-principles calculations are performed using the OpenMX code [24], which is based on density functional theory with the generalized gradient approximation (GGA) [25] and norm-conserving pseudopotentials [26]. The wave function is expressed by linear combination of pseudoatomic orbitals (LCAO). In structure optimization, standard basis sets are used: Ga7.0- $s3p2d2$ , Zn6.0S- $s3p2d1$ , N6.0- $s2p2d1$ , Si7.0- $s2p2d1$ , O6.0- $s2p2d1$ , H6.0- $s2p1$ , and Ru7.0- $s3p2d2$  for Ga, Zn, N, Si, O, H, and Ru atoms, respectively. The convergence criterion of  $1 \times 10^{-4}$  Hartree/Bohr is used. In band structure calculations, precise basis sets are used: Ga7.0- $s3p2d2f1$ , Zn6.0S- $s3p2d2f1$ , N6.0- $s3p2d2$ , Si7.0- $s3p3d2$ , O6.0- $s3p2d2$ , and H7.0- $s2p2d1$ .

To make a structure model of  $a$ -SiO<sub>2</sub>, melt-quenching classical molecular dynamics simulations are performed using BKS potentials [27–29]. The temperature is controlled using the Nosé-Poincaré thermostat [30–32].

## III. RESULTS AND DISCUSSIONS

### A. Hexagonal silica bilayer on $m$ -GaN

A material having small lattice mismatch with the  $m$ -GaN surface has the potential to be epitaxially grown on it. In this regard, a hexagonal silica bilayer ( $h$ -SiO<sub>2</sub> bilayer), which consists of two hexagonal Si<sub>2</sub>O<sub>3</sub> monolayers bridged by O atoms, is promising [33]. Figure 1(a) shows a rectangular

supercell of a freestanding  $h$ -SiO<sub>2</sub> bilayer optimized using first principles calculations with a  $6 \times 3 \times 1$   $k$ -grid. This supercell contains 8 Si atoms and 16 O atoms. The optimized lattice parameters in the  $c$  and  $a$  directions are  $c_{\text{hsb}} = 5.327$  Å and  $a_{\text{hsb}} = 9.226$  Å, respectively. Note that the length of the supercell in the  $m$  direction is fixed to be  $m_{\text{hsb}} = 42.000$  Å in structure optimization. The lattice parameters of the  $h$ -SiO<sub>2</sub> bilayer match well with those of a rectangular supercell of bulk  $m$ -GaN [Fig. 1(b)],  $c_{\text{GaN}} = 5.269$  Å and  $a_{\text{GaN}} = 9.693$  Å. Note that the optimized lattice parameter in the  $m$  direction is  $m_{\text{GaN}} = 5.601$  Å. The  $c$ ,  $a$ , and  $m$  axes are set to be along the [0001], [11 $\bar{2}$ 0], and [ $\bar{1}$ 100] directions of the GaN, respectively. A  $6 \times 3 \times 6$   $k$ -grid is used in the calculations of the bulk  $m$ -GaN. The average lattice mismatch of the  $h$ -SiO<sub>2</sub> bilayer with the  $m$ -GaN surface defined as  $\sqrt{c_{\text{hsb}}a_{\text{hsb}}/c_{\text{GaN}}a_{\text{GaN}}} - 1$  is  $-2\%$ . We point out that the epitaxial formation of an  $h$ -SiO<sub>2</sub> bilayer on a Ru(0001) surface was experimentally observed [33]. The computed lattice mismatch between  $h$ -SiO<sub>2</sub> and Ru(0001) is  $-3\%$ , which compares to that between  $h$ -SiO<sub>2</sub> and  $m$ -GaN. Thus we regard the  $h$ -SiO<sub>2</sub> bilayer as having the potential to be epitaxially grown on  $m$ -GaN.

To further examine the possibility for the  $h$ -SiO<sub>2</sub> bilayer being epitaxially grown on  $m$ -GaN, we compute the adhesion energy using a slab model illustrated in Fig. 2(a), which we call model A. It consists of an  $m$ -GaN slab sandwiched by two  $h$ -SiO<sub>2</sub> bilayers, Si<sub>8</sub>O<sub>16</sub>/(Ga<sub>6</sub>N<sub>6</sub>)<sub>16</sub>/Si<sub>8</sub>O<sub>16</sub>. The GaN slab consists of 16 GaN layers (about 43 Å thick). The atomic coordinates of this model are given in the Supplemental Material [34]. In optimizing the geometry, the lattice parameters in the  $c$  and  $a$  directions are fixed to the corresponding values of bulk GaN. The length of the supercell in the  $m$  direction is set to 84.000 Å. The length of the vacuum region is about 28 Å. A  $6 \times 3 \times 1$   $k$ -grid is used. The adhesion energy per Si<sub>8</sub>O<sub>16</sub> unit is defined as

$$e_{\text{adsorption}} = -(E_A - 2E_{\text{Si}_8\text{O}_{16}} - E_{(\text{Ga}_6\text{N}_6)_{16}})/2, \quad (1)$$

where  $E_A$  is the total energy of model A per supercell,  $E_{\text{Si}_8\text{O}_{16}}$  is the total energy of the freestanding  $h$ -SiO<sub>2</sub> per Si<sub>8</sub>O<sub>16</sub> unit, and  $E_{(\text{Ga}_6\text{N}_6)_{16}}$  is the total energy of the corresponding freestanding  $m$ -GaN slab per (Ga<sub>6</sub>N<sub>6</sub>)<sub>16</sub> unit. Note that 2 in the denominator accounts for the fact that the slab model has two epitaxial bilayers. The computed adhesion energy is 0.73 eV. The positive value suggests that the epitaxial formation of the  $h$ -SiO<sub>2</sub> bilayer on  $m$ -GaN is energetically favorable.

Figure 2(b) highlights the contact structure between the GaN slab and the upper epitaxial  $h$ -SiO<sub>2</sub> bilayer, which we call a type-A contact structure. It consists of the surface GaN layer and the Si<sub>2</sub>O<sub>3</sub> monolayer, which come in contact with each other. We refer to an interface with this contact structure as a type-A interface.

Every Ga atom in the surface GaN layer forms a bond with an O atom in the  $h$ -SiO<sub>2</sub> bilayer. The average length of the Ga-O bonds (2.08 Å) is longer than that of the Ga-O bonds in  $\beta$ -Ga<sub>2</sub>O<sub>3</sub> (1.97 Å). Two of three N atoms in the surface GaN layer form a bond with a Si atom in the  $h$ -SiO<sub>2</sub> bilayer. The average length of the N-Si bonds (2.00 Å) is longer than that of the N-Si bonds in  $\beta$ -Si<sub>3</sub>N<sub>4</sub> (1.76 Å). Due to the formation of the Ga-O and N-Si bonds, the O and Si atoms in the  $h$ -SiO<sub>2</sub> bilayer are three- and fivefold coordinated, respectively. The

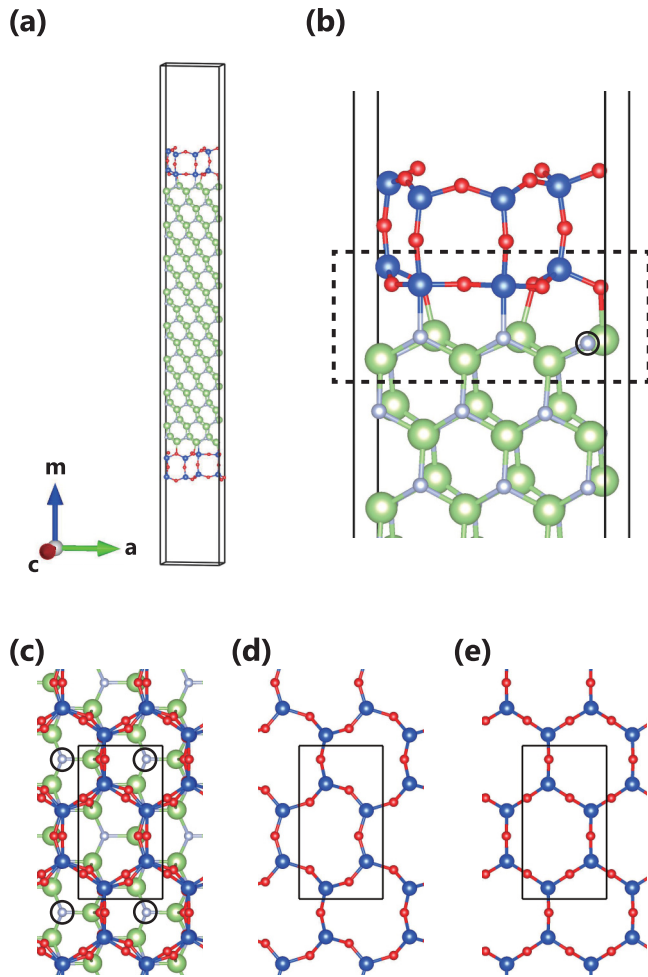


FIG. 2. Atomic structure of model A,  $\text{Si}_8\text{O}_{16}/(\text{Ga}_6\text{N}_6)/\text{Si}_8\text{O}_{16}$ . (a) Overall view. (b) Enlarged view. The  $h$ - $\text{SiO}_2$  bilayer consists of two  $\text{Si}_2\text{O}_3$  monolayers bridged by O atoms. The dashed square indicates the contact structure of the GaN/SiO<sub>2</sub> interface, which consists of the surface GaN layer and the  $\text{Si}_2\text{O}_3$  monolayer. We refer to this contact structure as a type-A contact structure. We also refer to an interface with this contact structure as a type-A interface. The Si atoms and the O atoms bonded to an N atom and a Ga atom, respectively, are overcoordinated. The circle indicates the tricoordinated N atom. Note that the bonds across the supercell are not shown. (c) Top view. Only the surface GaN layer and the epitaxial  $h$ - $\text{SiO}_2$  bilayer are shown. The circles indicate the tricoordinated N atoms. (d)  $\text{Si}_2\text{O}_3$  monolayer in contact with the  $m$ -GaN surface. (e)  $\text{Si}_2\text{O}_3$  monolayer away from the  $m$ -GaN surface.

overcoordinated atoms can be regarded as structure defects. However, these structure defects do not create states in the band gap as shown later.

The top view of the epitaxial  $h$ - $\text{SiO}_2$  bilayer and the surface GaN layer is illustrated in Fig. 2(c). The hexagonal rings of the  $\text{Si}_2\text{O}_3$  monolayer in contact with the GaN layer are highly distorted due to the formation of the Ga-O and N-Si bonds [Fig. 2(d)]. The distorted hexagonal rings resemble those of a freestanding  $\text{Si}_2\text{O}_3$  monolayer [35]. By contrast, the hexagonal rings of the  $\text{Si}_2\text{O}_3$  monolayer away from the GaN remain almost intact [Fig. 2(e)].

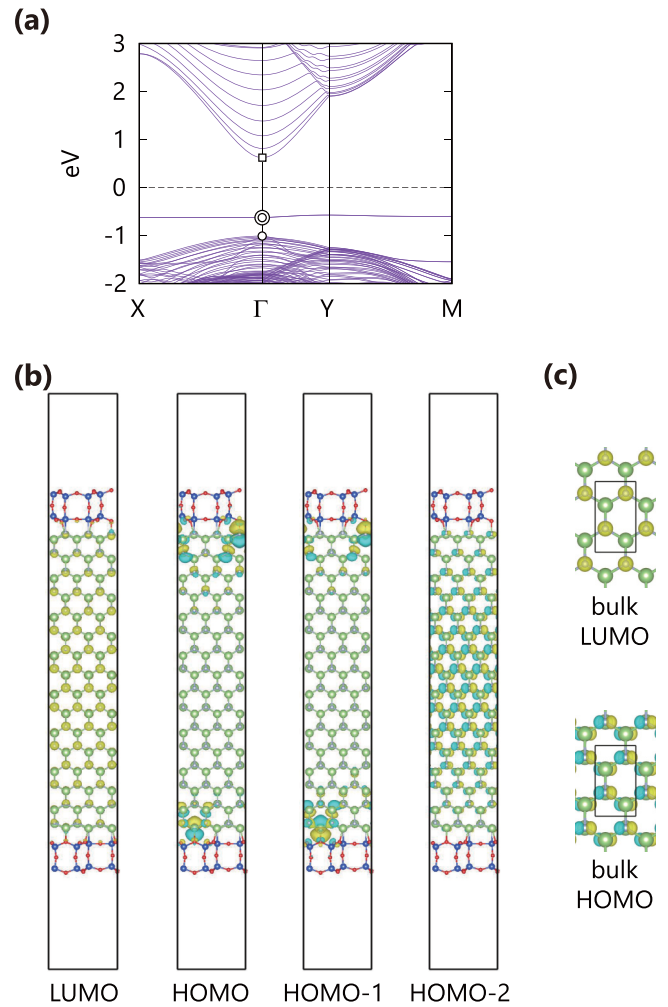


FIG. 3. Electronic structure of model A. (a) Band structure. The energy is measured from the Fermi level. The square, double circles, and circle indicate LUMO, HOMO and HOMO-1 and HOMO-2 at  $\Gamma$  point, respectively. (b) MOs at  $\Gamma$  point. The isovalue is  $\pm 0.014$  ( $\text{electron}^{1/2}/a_0$ ).  $a_0$  is the Bohr radius. (c) LUMO and HOMO at  $\Gamma$  point of bulk GaN for reference.

The band structure and molecular orbitals (MOs) at  $\Gamma$  point of model A are shown in Figs. 3(a) and 3(b), respectively. The lowest unoccupied MO (LUMO) at  $\Gamma$  point is bulklike, for it mainly consists of  $s$  orbitals of the N atoms as with LUMO at  $\Gamma$  point of bulk GaN [Fig. 3(c)]. The third highest occupied MO (HOMO-2) at  $\Gamma$  point is also bulklike, for it mainly consists of  $p_a$  orbitals of the N atoms. Here, the  $p_a$  orbital is the  $p$  orbital parallel to the  $a$  axis. Two nearly degenerate flat bands are formed in the band gap. They originate from the  $p_m$ -like dangling bonds of the two threefold coordinated N atoms, one in each GaN surface (see HOMO and HOMO-1 at  $\Gamma$  point). Note that it was reported that a clean  $m$ -GaN surface creates a similar occupied  $p_m$ -like dangling-bond band above the valence band of bulk GaN [21,22]. It was also reported that the threefold coordinated Ga atoms of the clean  $m$ -GaN surface create an unoccupied dangling-bond band below the conduction band of bulk GaN. By contrast, model A does not have such Ga dangling-bond bands, for all the dangling bonds

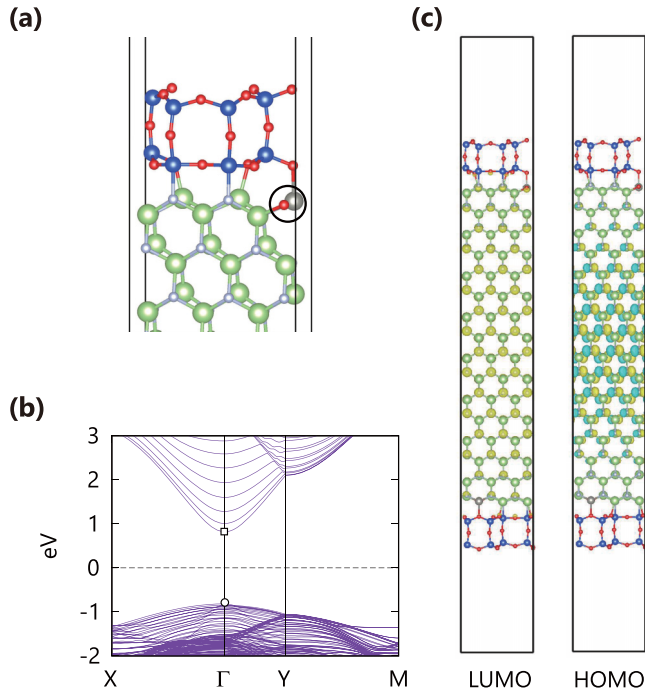


FIG. 4. Model B1,  $\text{Si}_8\text{O}_{16}/(\text{ZnOGa}_5\text{N}_5)(\text{Ga}_6\text{N}_6)_{14}(\text{ZnOGa}_5\text{N}_5)/\text{Si}_8\text{O}_{16}$ . (a) Atomic structure around the upper type-B interface. The brown sphere represents a Zn atom. The doped Zn and O atoms are circled. (b) Band structure. (c) LUMO and HOMO at  $\Gamma$  point.

of the surface Ga atoms are passivated by the O atoms of the  $h$ - $\text{SiO}_2$  bilayers.

### B. Effect of ZnO doping on the band structure

The type-A interface is not suitable for the application to power transistors, for it would create states in the band gap of GaN. To avoid the formation of in-gap states, we examine the effect of ZnO doping on the band structure. As illustrated in Fig. 4(a), we first replace the threefold coordinated N atom of each interface with an O atom. To meet the electron counting rule, we then replace a Ga atom of each interface with a Zn atom. We refer to the resulting contact structure as a type-B contact structure. We also refer to the resulting slab model as model B1,  $\text{Si}_8\text{O}_{16}/(\text{ZnOGa}_5\text{N}_5)(\text{Ga}_6\text{N}_6)_{14}(\text{ZnOGa}_5\text{N}_5)/\text{Si}_8\text{O}_{16}$ . The atomic coordinates of this model are given in the Supplemental Material [34]. Figures 4(b) and 4(c) show that both CBM and VBM of model B1 originate from the GaN.

To explain the reason why in-gap states are absent in model B1, the projected density of states (PDOS) of the  $p_m^{\text{N}}$  orbitals in model A and of the  $p_m^{\text{O}}$  orbitals in model B1 are shown in Figs. 5(a) and 5(b), respectively. Here,  $p_m^{\text{N}}$  and  $p_m^{\text{O}}$  are the  $p_m$  orbitals of the threefold coordinated anions, N and O atoms, respectively. The  $p_m^{\text{N}}$ -orbitals PDOS has a sharp peak in the band gap of the GaN, indicating that the  $p_m^{\text{N}}$  orbitals hardly hybridize with the GaN crystal orbitals. This result can be confirmed by Fig. 3, which shows that nearly isolated  $p_m$  states occur in the band gap of the GaN. By contrast, the  $p_m^{\text{O}}$ -orbitals PDOS has a broad peak inside the valence band of the GaN, indicating that the  $p_m^{\text{O}}$  orbitals substantially hybridize with the

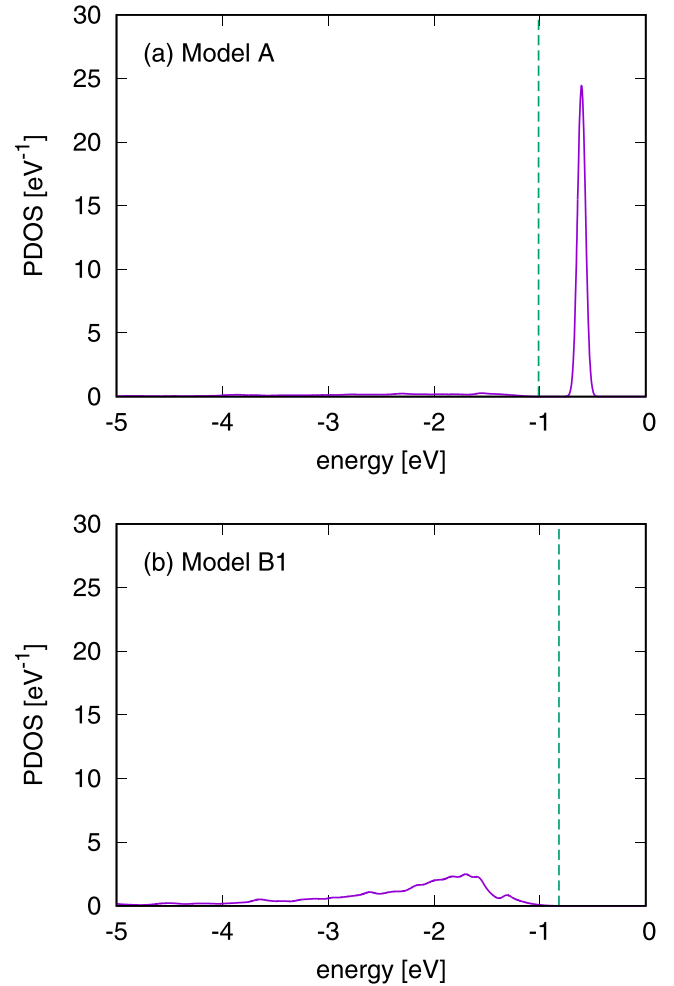


FIG. 5. Projected density of states (PDOS) of the threefold coordinated anion  $p_m$  orbitals. (a) The  $p_m$  orbitals of the threefold coordinated N atoms in model A (solid line). The vertical dashed line indicates the position of the valence band edge of the GaN. (b) The  $p_m$  orbitals of the corresponding doped O atoms in model B1. PDOS is calculated using the Gaussian smearing with a smearing of 0.04 eV.

GaN crystal orbitals. The differences in PDOS suggest that the decrease in  $p_m$  orbital energy  $\langle p_m | H_{\text{KS}} | p_m \rangle$  of the threefold coordinated anion is the reason why model B1 does not have nearly isolated  $p_m$  states in the band gap.

Note that the structure change caused by ZnO doping is so small that the local structure around the O-Zn pair in model B1 and the N-Ga pair in model A are essentially the same. In particular, the doped O atom in model B1 remains threefold coordinated. Because of the small structure change, the band structures of model B1 before and after geometry optimization are essentially the same. In other words, geometry modification does not play a key role in the removal of in-gap states.

### C. Relative stability of ZnO doped interfaces

We examine the relative stability of the type-B interface, the type-A interface, and other competing structures in terms of the doping energy per ZnO pair which is defined as

$$e_{\text{doping}} = -[E_X - E_A + n(\mu_{\text{Ga}} + \mu_{\text{N}} - \mu_{\text{Zn}} - \mu_{\text{O}})]/2. \quad (2)$$

Here,  $E_X$  is the total energy of model X per supercell,  $n$  is the number of doped ZnO pairs, and  $\mu_Y$  is the chemical potential of the reservoir of element Y. The positive value of doping energy indicates that replacing GaN pairs with ZnO pairs is favorable. Since we assume that the system is in equilibrium with bulk GaN,  $\mu_{\text{Ga}} + \mu_{\text{N}} = E_{\text{GaN}}$  [36]. Here,  $E_{\text{GaN}}$  is the total energy per two-atom unit of bulk GaN. We choose the total energy per atom of hexagonal-closed-packed Zn ( $E_{\text{Zn}}$ ) and that of an O<sub>2</sub> molecule ( $E_{\text{O}}$ ) as the upper bounds of  $\mu_{\text{Zn}}$  and  $\mu_{\text{O}}$ , respectively. We assume that model A is in equilibrium in the absence of zinc:  $\mu_{\text{Si}} + 2\mu_{\text{O}} = (E_{\text{A}} - 96\mu_{\text{Ga}} - 96\mu_{\text{N}})/16$ . We choose the total energy per atom of the Si crystal ( $E_{\text{Si}}$ ) as the upper bound of  $\mu_{\text{Si}}$ . Although  $\mu_{\text{Si}}$  does not appear in Eq. (2), its upper limit sets the lower limit of  $\mu_{\text{O}}$  as  $\mu_{\text{O}}(\text{min}) = [(E_{\text{A}} - 96\mu_{\text{Ga}} - 96\mu_{\text{N}})/16 - E_{\text{Si}}]/2$ .

Since it is practically impossible to examine all competing structures, we examine a total of 32 representative competitors that are made by modifying model B1. The competing models are classified into five classes. The class 1 comprises seven models made by interchanging the doped Zn atom of each type-B interface with a Ga atom in the surface GaN layer or the layer next to the surface. Note that a total of ten models are made by this type of modification but only seven are independent by symmetry. The class 2 comprises four models made by interchanging the doped Zn atom of each type-B interface with a Si atom. The class 3 comprises seven models made by interchanging the doped O atom of each type-B interface with an N atom in the surface GaN layer or the layer next to the surface. The class 4 comprises seven models made by interchanging the doped ZnO pair of each type-B interface with a GaN pair in the surface GaN layer or the layer next to the surface. The class 5 comprises seven models made by doping one ZnO pair with each type-B interface.

We compare the doping energy of model B1 with those of the competitors, and find that there exists a region on the  $\Delta\mu_{\text{Zn}}\Delta\mu_{\text{O}}$  plane in which model B1 is the most stable as illustrated in Fig. 6(a). Here,  $\Delta\mu_{\text{Zn}} = \mu_{\text{Zn}} - \mu_{\text{Zn}}(\text{max})$  and  $\Delta\mu_{\text{O}} = \mu_{\text{O}} - \mu_{\text{O}}(\text{max})$ . The result suggests that the type-B interface is the most favorable when the chemical potentials of zinc and oxygen are not too low and not too high so that they fall within the blue region of Fig. 6(a). In other words, controlling the amount of zinc and oxygen is key to the formation of the type-B interface. For the reader's convenience, Fig. 6(b) shows the doping energies as a function of  $\Delta\mu_{\text{Zn}}$  at  $\Delta\mu_{\text{O}} = [\mu_{\text{O}}(\text{min}) - \mu_{\text{O}}(\text{max})]/2$ . When little zinc is available ( $\Delta\mu_{\text{Zn}} < -0.81$  eV), ZnO doping is unfavorable. When zinc abounds ( $-0.33$  eV  $< \Delta\mu_{\text{Zn}}$ ), doping each interface with more than one ZnO pair becomes more favorable. When a proper amount of zinc is available ( $-0.83$  eV  $\leq \Delta\mu_{\text{Zn}} \leq -0.38$  eV), model B1 is the most stable.

#### D. Interface between *m*-GaN and *a*-SiO<sub>2</sub>

From the results of model B1, we expect that the *m*-GaN/*a*-SiO<sub>2</sub> interface with the type-B contact structure would create no states in the band gap of the *m*-GaN. However, it is unknown whether it is possible to connect *a*-SiO<sub>2</sub> smoothly to *m*-GaN through the type-B contact structure. It is also unknown whether it is possible to form the type-B *m*-GaN/*a*-SiO<sub>2</sub> interface that has a straddling band gap. To elucidate

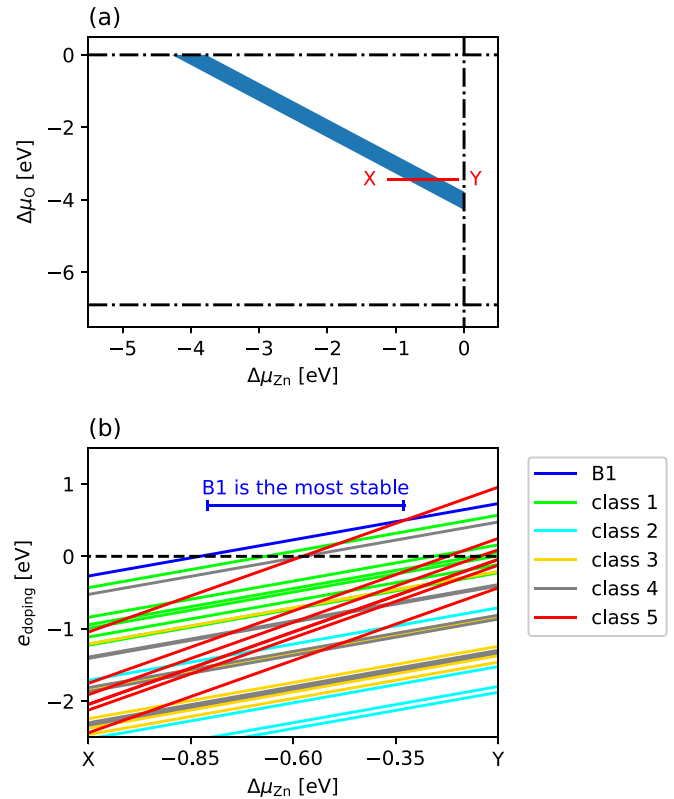


FIG. 6. Stabilities of models as a function of the zinc and oxygen chemical potentials,  $\Delta\mu_{\text{Zn}}$  and  $\Delta\mu_{\text{O}}$ , respectively. (a) The blue region represents the condition in which model B1 is the most stable. The horizontal dash-dotted lines indicate the upper and lower limits of the oxygen chemical potential. The vertical dash-dotted line indicates the upper limit of the zinc chemical potential. (b) The doping energies of model B1 and the competitors of the classes from 1 to 5. The energies are calculated along the red segment XY in (a).

these points, we attempt to make a superlattice model of the type-B *m*-GaN/*a*-SiO<sub>2</sub> interface by exploiting epitaxial *h*-SiO<sub>2</sub> bilayers as follows (Fig. 7).

*Step (a)* [Fig. 7(a)]: We start with an eight-layer *m*-GaN slab doped with zinc and oxygen to which *h*-SiO<sub>2</sub> bilayers are connected through type-B interfaces. The supercell is made by duplicating the primitive cell of the type-B interfaces in the *c* and *a* directions. Periodic boundary conditions are applied in all three directions.

*Step (b)* [Fig. 7(b)]: We remove all the atoms except for the Si<sub>2</sub>O<sub>3</sub> monolayers in contact with the GaN slab.

*Step (c)* [Fig. 7(c)]: We place Si and O atoms randomly into the outside region. The supercell contains a total of 44 Si atoms and 88 O atoms.

*Step (d)* [Fig. 7(d)]: We use melt-quenching classical molecular dynamics simulations to make *a*-SiO<sub>2</sub>. The system is equilibrated at 4000 K, cooled down to 1000 K at a rate of 100 K/ps, and then equilibrated at 300 K. In this process, the Si<sub>2</sub>O<sub>3</sub> monolayers are fixed as boundary conditions for *a*-SiO<sub>2</sub>. The other atoms spontaneously rearrange themselves to adapt to the boundary conditions. The resulting *a*-SiO<sub>2</sub> has no dangling bonds.

*Step (e)* [Fig. 7(e)]: We put the GaN slab back into its original position. Since the Si<sub>2</sub>O<sub>3</sub> monolayers are fixed in

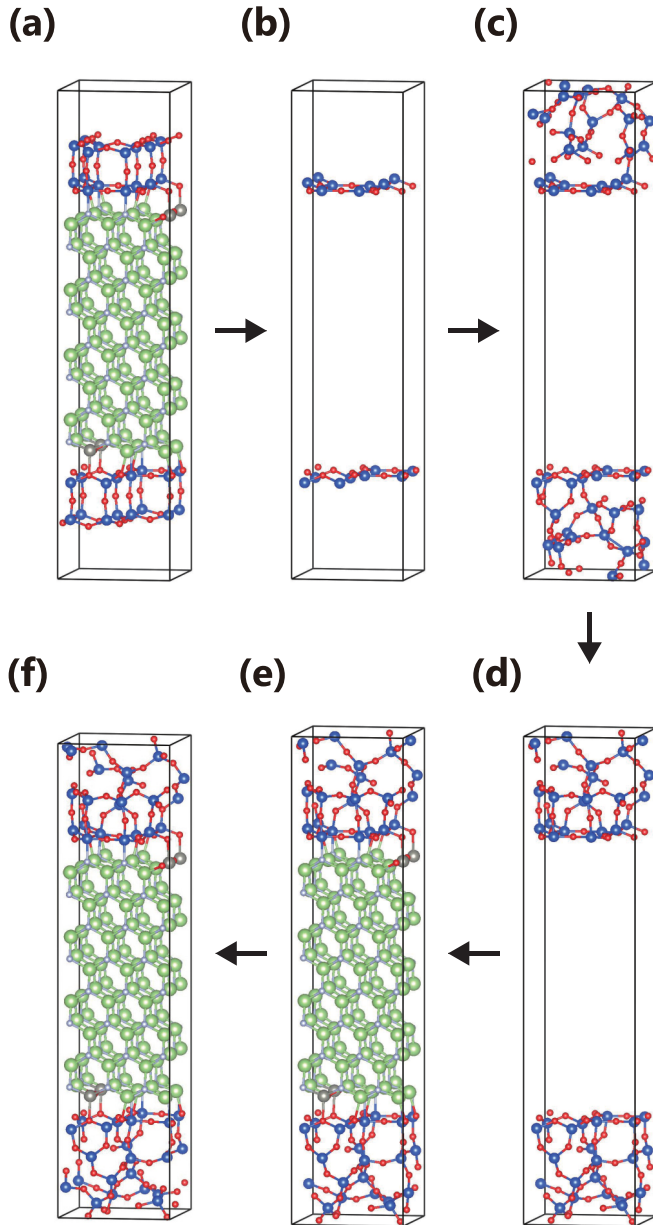


FIG. 7. Steps to making model B2. (a) We start with  $h$ -SiO<sub>2</sub> bilayers connected through type-B interfaces to a ZnO-doped eight-layer GaN slab. The supercell is made by duplicating the primitive cell of the type-B interfaces in the  $c$  and  $a$  directions. Periodic boundary conditions are applied in all the three directions. (b) The atoms are removed except for the Si<sub>2</sub>O<sub>3</sub> monolayers in contact with the ZnO-doped GaN slab. (c) Si and O atoms are randomly placed. The supercell contains a total of 44 Si atoms and 88 O atoms. (d) Amorphous SiO<sub>2</sub> is made using melt-quenching classical molecular dynamics simulations. In this process, the Si<sub>2</sub>O<sub>3</sub> monolayers are fixed. The system is equilibrated at 4000 K, cooled down to 1000 K at a rate of 100 K/ps, and then equilibrated at 300 K. The resulting  $a$ -SiO<sub>2</sub> has no dangling bonds. (e) The ZnO-doped GaN slab is inserted. (f) The structure is optimized using first principles calculations with a  $3 \times 3 \times 1$   $k$ -grid.

the melt-quenching classical molecular dynamics simulations, the  $a$ -SiO<sub>2</sub> and  $m$ -GaN form type-B contact structures. Consequently, at each interface, the contact structure connects

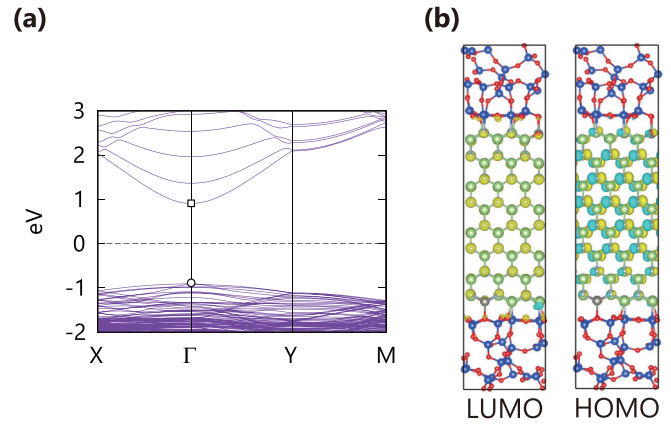


FIG. 8. Electronic structure of model B2. (a) Band structure. (b) LUMO and HOMO at  $\Gamma$  point.

the random structure of the  $a$ -SiO<sub>2</sub> smoothly to the regular structure of the crystalline GaN.

*Step (f)* [Fig. 7(f)]: We optimize the structure using first principles calculations with a  $3 \times 3 \times 1$   $k$ -grid. The density of the  $a$ -SiO<sub>2</sub> is 2.09 g/cm<sup>3</sup>, which is consistent with the range of experimental densities: from 1.90 to 2.20 g/cm<sup>3</sup> [37]. We refer to the model thus obtained as model B2. The atomic coordinates of this model are given in the Supplemental Material [34]. Note that models B1 and B2 both contain two type-B interfaces.

Model B2 suggests that the random structure of  $a$ -SiO<sub>2</sub> can smoothly connect to the ordered structure of  $m$ -GaN. Moreover, Fig. 8 shows that the characteristics of LUMO and HOMO at  $\Gamma$  point of model B2 are both bulklike. Consequently, the interface that has a straddling band gap without in-gap states is obtained. To explicitly illustrate the band alignment, we examine the position dependence of the projected density of states (PDOS). For this purpose, we define PPDOS( $E, z$ ) as

$$\text{PPDOS}(E, z) = \sum_i \frac{1}{\sqrt{2\pi\sigma^2}} \exp\left\{-\frac{[z(i) - z]^2}{2\sigma^2}\right\} \text{PDOS}_i(E). \quad (3)$$

Here,  $E$  is the energy,  $z$  is the  $z$  coordinate,  $\sigma$  is a smearing parameter which we set at 1 Å,  $z(i)$  is the  $z$  coordinate of atom  $i$ , and  $\text{PDOS}_i(E)$  is the projected density of states of atom  $i$ . Note that

$$\text{DOS}(E) = \int \text{PPDOS}(E, z) dz, \quad (4)$$

where  $\text{DOS}(E)$  is the density of states. Figure 9 illustrates that the conduction and valence band edges of the GaN lie in between those of the  $a$ -SiO<sub>2</sub>. Thus the  $m$ -GaN/ $a$ -SiO<sub>2</sub> interface of type B is confirmed to have a straddling gap.

It is known that the GGA method describes valence bands well, but it underestimates the band gap energy. Therefore, we estimate the experimental conduction band edges of the type-B interface by combining the calculated energies of the valence band edges and the experimental band gap energies. Figure 9 shows that the calculated valence band edge of the  $a$ -SiO<sub>2</sub> lies 0.8 eV below that of the GaN. The experimental

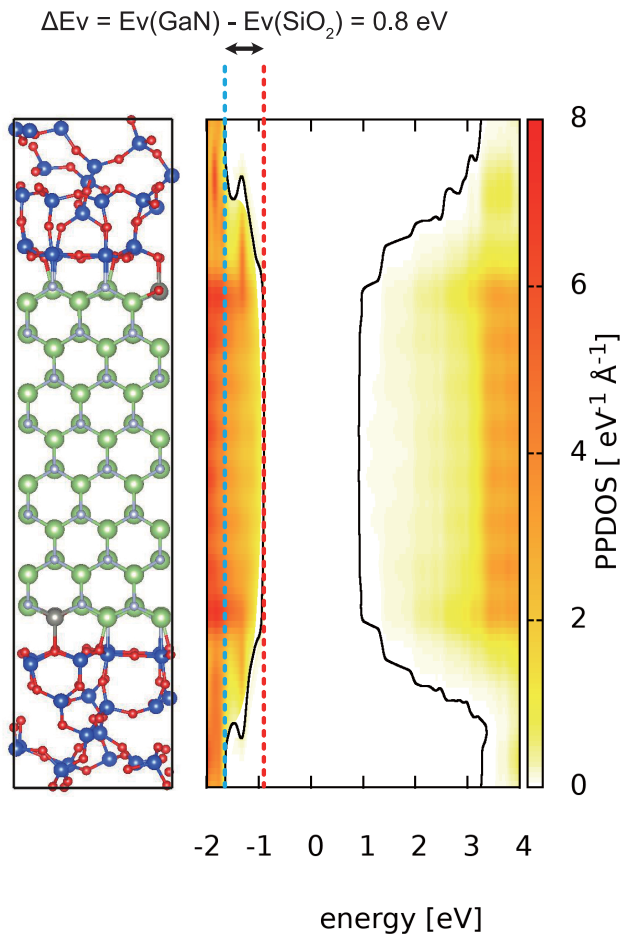


FIG. 9. Position dependence of the PDOS (PPDOS). The solid lines above and below 0 eV are respectively the contour lines whose energies in the GaN region agree with the energies of CBM and VBM calculated from the band structure shown in Fig. 8. Therefore, these lines show the position dependence of the band edges. The red and blue dashed lines indicate the energies of the valence band edges of the GaN and *a*-SiO<sub>2</sub>,  $E_v(\text{GaN})$  and  $E_v(a\text{-SiO}_2)$ , respectively.

band gaps of GaN and *a*-SiO<sub>2</sub> are 3.4 and 8.95 eV, respectively [8]. From these values, the experimental conduction band edge of *a*-SiO<sub>2</sub> is estimated to lie 4.75 (= 8.95 – 3.4 – 0.8) eV above that of GaN. This suggests that the *m*-GaN/*a*-SiO<sub>2</sub> interface of type B has a straddling gap.

The removal of in-gap states near VBM is a challenge for the application of GaN. Our result that the occupied in-gap states near VBM can be removed by ZnO doping does not suffer from GGA's poor description of conduction bands.

Next we discuss the relative positions of unoccupied states. It is known that the calculation using the Heyd-Scuseria-Ernzerhof (HSE) hybrid functional reproduces the band gap energy well [38]. HSE calculations showed that a clean *m*-GaN surface has unoccupied states derived from the dangling bonds of surface Ga atoms below the conduction band of bulk GaN [22,23] and that a hydrogen-saturated *m*-GaN surface does not create such in-gap states. GGA calculations including ours are successful in reproducing these HSE results [22], sug-

gesting that the GGA method describes the relative positions of unoccupied states. As with the hydrogen-saturated *m*-GaN surface, in our *m*-GaN/*a*-SiO<sub>2</sub> interface model, the dangling bonds of Ga atoms, which are possible sources of unoccupied in-gap states, are passivated by O atoms of *a*-SiO<sub>2</sub>. In fact, our interface model does not have unoccupied in-gap states as shown in Fig. 8. Consequently, we propose that the *m*-GaN/*a*-SiO<sub>2</sub> interface of type B does not create in-gap states.

The *m*-GaN/*a*-SiO<sub>2</sub> interface of type B, which has a straddling gap and does not create in-gap states, would be suitable for the application to power transistors. Although we examine other *m*-GaN/*a*-SiO<sub>2</sub> interfaces (see Supplemental Material [34]), none of them have band structures more suitable than the type-B interface.

Similarities in structure between models B1 and B2 suggest that an epitaxial *h*-SiO<sub>2</sub> bilayer can serve as a seed for a type-B *m*-GaN/*a*-SiO<sub>2</sub> interface. A possible approach to experimentally form this type of interface is deposition of *a*-SiO<sub>2</sub> onto an *h*-SiO<sub>2</sub> bilayer epitaxially grown on an *m*-GaN surface doped with zinc and oxygen. If the Si<sub>2</sub>O<sub>3</sub> monolayer away from the GaN and the bridging O atoms are merged with the deposited *a*-SiO<sub>2</sub> without damaging the Si<sub>2</sub>O<sub>3</sub> monolayer in contact with the GaN, then the type-B *m*-GaN/*a*-SiO<sub>2</sub> interface would be formed.

#### IV. CONCLUSION

For the application of GaN to power transistors, the interface between GaN and the gate insulator needs to meet the following requirements: (1) both CBM and VBM originate from the GaN and (2) the formation of in-gap states is minimized. Our calculations have shown that the type-B *m*-GaN/*a*-SiO<sub>2</sub> interface meets these requirements. A clean *m*-GaN surface has in-gap states derived from the dangling bonds of the surface Ga and N atoms. At the type-B interface, the Ga dangling bonds are passivated by O atoms of *a*-SiO<sub>2</sub>, two-thirds of the N dangling bonds are passivated by Si atoms of *a*-SiO<sub>2</sub>, and the pairs of a Ga atom and a threefold coordinated N atom are replaced with ZnO pairs. As a result, the type-B interface does not create in-gap states. A possible approach to experimentally synthesize the type-B interface is deposition of *a*-SiO<sub>2</sub> onto an *h*-SiO<sub>2</sub> bilayer epitaxially grown on an *m*-GaN surface doped with zinc and oxygen. It has been demonstrated that the contact structure of the *m*-GaN/*a*-SiO<sub>2</sub> interface is a key determinant of the nature of interface band structure. We propose that the complex problem of designing semiconductor/insulator interfaces can be reduced to the simpler problem of designing ultrathin epitaxial insulators on the semiconductor surface. Our findings would help not only improve the performance of GaN-based transistors, but also design semiconductor/insulator interfaces in general.

#### ACKNOWLEDGMENTS

GDIS [39] was used to construct the structure models. VESTA [40] was used to illustrate the structure models. A part of this work is based on results obtained from a project, No. JPNP10022, commissioned by the New Energy and Industrial Technology Development Organization (NEDO).

- [1] F. Zaera, Probing liquid/solid interfaces at the molecular level, *Chem. Rev.* **112**, 2920 (2012).
- [2] F. Ernst, Metal-oxide interfaces, *Mater. Sci. Eng.: R: Rep.* **14**, 97 (1995).
- [3] P. G. De Gennes and C. Taupin, Microemulsions and the flexibility of oil/water interfaces, *J. Phys. Chem.* **86**, 2294 (1982).
- [4] G. D. Wilk, R. M. Wallace, and J. M. Anthony, High-k gate dielectrics: Current status and materials properties considerations, *J. Appl. Phys.* **89**, 5243 (2001).
- [5] E. H. Poindexter, G. J. Gerardi, M. Rueckel, P. J. Caplan, N. M. Johnson, and D. K. Biegelsen, Electronic traps and Pb centers at the Si/SiO<sub>2</sub> interface: Band-gap energy distribution, *J. Appl. Phys.* **56**, 2844 (1984).
- [6] A. Lidow, J. Strydom, M. d. Rooij, and D. Reusch, *GaN Transistors for Efficient Power Conversion* (Wiley, New York, 2014).
- [7] M. Placidi, A. Constant, A. Fontseré, E. Pausas, I. Cortes, Y. Cordier, N. Mestres, R. Pérez, M. Zabala, J. Millán, P. Godignon, and A. Pérez-Tomás, Deposited thin SiO<sub>2</sub> for gate oxide on n-type and p-type GaN, *J. Electrochem. Soc.* **157**, H1008 (2010).
- [8] N. X. Truyen, N. Taoka, A. Ohta, K. Makihara, H. Yamada, T. Takahashi, M. Ikeda, M. Shimizu, and S. Miyazaki, High thermal stability of abrupt SiO<sub>2</sub>/GaN interface with low interface state density, *Jpn. J. Appl. Phys.* **57**, 04FG11 (2018).
- [9] N. X. Truyen, N. Taoka, A. Ohta, K. Makihara, H. Yamada, T. Takahashi, M. Ikeda, M. Shimizu, and S. Miyazaki, Interface properties of SiO<sub>2</sub>/GaN structures formed by chemical vapor deposition with remote oxygen plasma mixed with Ar or He, *Jpn. J. Appl. Phys.* **57**, 06KA01 (2018).
- [10] A. Ohta, N. X. Truyen, N. Fujimura, M. Ikeda, K. Makihara, and S. Miyazaki, Total photoelectron yield spectroscopy of energy distribution of electronic states density at GaN surface and SiO<sub>2</sub>/GaN interface, *Jpn. J. Appl. Phys.* **57**, 06KA08 (2018).
- [11] Y. Tu and J. Tersoff, Structure and Energetics of the Si-SiO<sub>2</sub> Interface, *Phys. Rev. Lett.* **84**, 4393 (2000).
- [12] A. Ourmazd, D. W. Taylor, J. A. Rentschler, and J. Bevk, Si→SiO<sub>2</sub> Transformation: Interfacial Structure and Mechanism, *Phys. Rev. Lett.* **59**, 213 (1987).
- [13] N. Ikarashi, K. Watanabe, and Y. Miyamoto, High-resolution transmission electron microscopy of an atomic structure at a Si(001) oxidation front, *Phys. Rev. B* **62**, 15989 (2000).
- [14] R. Therrien, G. Lucovsky, and R. Davis, Charge redistribution at GaN-Ga<sub>2</sub>O<sub>3</sub> interfaces: A microscopic mechanism for low defect density interfaces in remote-plasma-processed MoS devices prepared on polar GaN faces, *Appl. Surf. Sci.* **166**, 513 (2000).
- [15] K. Mitsuishi, K. Kimoto, Y. Irokawa, T. Suzuki, K. Yuge, T. Nabatame, S. Takashima, K. Ueno, M. Edo, K. Nakagawa, and Y. Koide, Electron microscopy studies of the intermediate layers at the SiO<sub>2</sub>/GaN interface, *Jpn. J. Appl. Phys.* **56**, 110312 (2017).
- [16] Y. Irokawa, K. Mitsuishi, T. Nabatame, K. Kimoto, and Y. Koide, Investigation of intermediate layers in oxides/GaN(0001) by electron microscopy, *Jpn. J. Appl. Phys.* **57**, 118003 (2018).
- [17] K. Nishio, T. Yayama, T. Miyazaki, N. Taoka, and M. Shimizu, Ultrathin silicon oxynitride layer on GaN for dangling-bond-free GaN/insulator interface, *Sci. Rep.* **8**, 1391 (2018).
- [18] J. Bernhardt, J. Schardt, U. Starke, and K. Heinz, Epitaxially ideal oxide-semiconductor interfaces: Silicate adlayers on hexagonal (0001) and (000 $\bar{1}$ ) SiC surfaces, *Appl. Phys. Lett.* **74**, 1084 (1999).
- [19] T. Shirasawa, K. Hayashi, S. Mizuno, S. Tanaka, K. Nakatsuji, F. Komori, and H. Tochiyama, Epitaxial Silicon Oxynitride Layer on a 6H-SiC(0001) Surface, *Phys. Rev. Lett.* **98**, 136105 (2007).
- [20] R. A. Khadar, C. Liu, R. Soleimanzadeh, and E. Matioli, Fully vertical GaN-on-Si power MOSFETs, *IEEE Electron Device Lett.* **40**, 443 (2019).
- [21] J. E. Northrup and J. Neugebauer, Theory of GaN(10 $\bar{1}$ 0) and (11 $\bar{2}$ 0) surfaces, *Phys. Rev. B* **53**, R10477 (1996).
- [22] M. Landmann, E. Rauls, W. G. Schmidt, M. D. Neumann, E. Speiser, and N. Esser, GaN *m*-plane: Atomic structure, surface bands, and optical response, *Phys. Rev. B* **91**, 035302 (2015).
- [23] L. Lymperakis, J. Neugebauer, M. Himmerlich, S. Krischok, M. Rink, J. Kröger, and V. M. Polyakov, Adsorption and desorption of hydrogen at nonpolar GaN(1 $\bar{1}$ 00) surfaces: Kinetics and impact on surface vibrational and electronic properties, *Phys. Rev. B* **95**, 195314 (2017).
- [24] <http://www.openmx-square.org/>.
- [25] J. P. Perdew, K. Burke, and M. Ernzerhof, Generalized Gradient Approximation Made Simple, *Phys. Rev. Lett.* **77**, 3865 (1996).
- [26] I. Morrison, D. M. Bylander, and L. Kleinman, Nonlocal Hermitian norm-conserving Vanderbilt pseudopotential, *Phys. Rev. B* **47**, 6728 (1993).
- [27] B. W. H. van Beest, G. J. Kramer, and R. A. van Santen, Force Fields for Silicas and Aluminophosphates Based on *Ab Initio* Calculations, *Phys. Rev. Lett.* **64**, 1955 (1990).
- [28] J. Yu, R. Devanathan, and W. J. Weber, Unified interatomic potential for zircon, zirconia and silica systems, *J. Mater. Chem.* **19**, 3923 (2009).
- [29] K. Nishio, T. Miyazaki, and H. Nakamura, Universal Medium-Range Order of Amorphous Metal Oxides, *Phys. Rev. Lett.* **111**, 155502 (2013).
- [30] S. D. Bond, B. J. Leimkuhler, and B. B. Laird, The Nosé-Poincaré method for constant temperature molecular dynamics, *J. Comput. Phys.* **151**, 114 (1999).
- [31] S. Nosé, An improved symplectic integrator for Nosé-Poincaré thermostat, *J. Phys. Soc. Jpn.* **70**, 75 (2001).
- [32] K. Nishio, A. K. A. Lu, and T. Miyazaki, Entropy-driven dicosahedral short-range order in simple liquids and glasses, *Phys. Rev. E* **99**, 022121 (2019).
- [33] D. Löffler, J. J. Uhlrich, M. Baron, B. Yang, X. Yu, L. Lichtenstein, L. Heinke, C. Büchner, M. Heyde, S. Shaikhutdinov, H.-J. Freund, R. Włodarczyk, M. Sierka, and J. Sauer, Growth and Structure of Crystalline Silica Sheet on Ru(0001), *Phys. Rev. Lett.* **105**, 146104 (2010).
- [34] See Supplemental Material at <http://link.aps.org/supplemental/10.1103/PhysRevMaterials.5.104601> for the atomic coordinates of models A, B1, and B2.
- [35] V. O. Özçelik, S. Cahangirov, and S. Ciraci, Stable Single-Layer Honeycomblike Structure of Silica, *Phys. Rev. Lett.* **112**, 246803 (2014).
- [36] G.-X. Qian, R. M. Martin, and D. J. Chadi, First-principles study of the atomic reconstructions and energies of Ga- and As-stabilized GaAs(100) surfaces, *Phys. Rev. B* **38**, 7649 (1988).
- [37] Silica, amorphous [mak value documentation, 1991], in *The MAK-Collection for Occupational Health and Safety* (American

- Cancer Society, 2012), pp. 158–179, <https://onlinelibrary.wiley.com/doi/pdf/10.1002/3527600418.mb763186e0002>.
- [38] J. Heyd, G. E. Scuseria, and M. Ernzerhof, Hybrid functionals based on a screened Coulomb potential, *J. Chem. Phys.* **118**, 8207 (2003).
- [39] <http://gdis.sourceforge.net/index.html/>.
- [40] K. Momma and F. Izumi, VESTA3 for three-dimensional visualization of crystal, volumetric and morphology data, *J. Appl. Crystallogr.* **44**, 1272 (2011).